

---

# STaRFormer: Semi-Supervised Task-Informed Representation Learning via Dynamic Attention-Based Regional Masking for Sequential Data

---

Maximilian Forstehäusler<sup>1,2</sup> Daniel Külzer<sup>1</sup> Christos Anagnostopoulos<sup>2</sup>  
 Shameem Puthiya Parambath<sup>2</sup> Natascha Weber<sup>1</sup>  
<sup>1</sup>BMW Group <sup>2</sup>University of Glasgow  
 maximilian.forstehaeusler@bmw.de,  
 m.forstehaeusler.1@research.gla.ac.uk,  
 {daniel.kuelzer, natascha.weber}@bmwgroup.com,  
 {Christos.Anagnostopoulos, Sham.Puthiya}@glasgow.ac.uk

## Abstract

Accurate predictions using sequential spatiotemporal data are crucial for various applications. Utilizing real-world data, we aim to learn the intent of a smart device user within confined areas of a vehicle’s surroundings. However, in real-world scenarios, environmental factors and sensor limitations result in non-stationary and irregularly sampled data, posing significant challenges. To address these issues, we developed a Transformer-based approach, STaRFormer, which serves as a universal framework for sequential modeling. STaRFormer employs a novel, dynamic attention-based regional masking scheme combined with semi-supervised contrastive learning to enhance task-specific latent representations. Comprehensive experiments on 15 datasets varying in types (including non-stationary and irregularly sampled), domains, sequence lengths, training samples, and applications, demonstrate the efficacy and practicality of STaRFormer. We achieve notable improvements over state-of-the-art approaches. Code and data will be made available.

## 1 Introduction

Advancements in machine learning architectures, such as Long Short-Term Memory (LSTM) [1] and Transformer [2], have enhanced the ability to model sequential data. However, these algorithms typically assume that the data is fully observed, stationary, and sampled at regular intervals [3]. In reality, sensor technology and external conditions often influence data collection, leading to non-stationary and irregularly sampled time series. For instance, in the automotive industry, manufacturers have recently integrated Ultra-Wideband (UWB) and Bluetooth Low-Energy (BLE) technologies to enhance the Digital Key (DK) [4–8]. This integration ensures precise and secure vehicle access along with applications for connected vehicles. Precise localization is achieved by performing time-of-flight calculations between each UWB anchor in a vehicle and a smart device, leveraging UWB’s  $2ns$  pulse duration [9]. However, the measuring algorithm for UWB ranging can result in irregularly recorded time-of-flight calculations, leading to irregularly sampled time series. When employing real-world trajectory data, created by the smart device carrier, to develop algorithms for predicting their intent, external factors such as signal interference or the position of smart devices can affect accuracy and introduce non-stationarity. In the real-world Digital Key Trajectories (DKT) dataset provided by our industrial partner, we confirmed, by Kwiatkowski–Phillips–Schmidt–Shin (KPSS) and augmented Dickey-Fuller (ADF) tests, that approximately 79% is non-stationary.

Deviating from the traditional time series learning paradigm of predicting future values from past observations, we focus on predicting intent from trajectories. Trajectories, i.e., spatiotemporal multivariate time series, involve variables such as latitude, longitude, altitude, and speed, and are often irregular. Similarly, factors such as weather conditions, geographical barriers, sensor availability, and device malfunctions [10] can result in non-stationary characteristics, which aligns with the DKT data. Although several solutions exist to address these issues, they require substantial prior knowledge and effort in model selection [11–20]. To address these challenges, we develop a versatile framework, STaRFormer, that effectively models time series with the aforementioned characteristics while being applicable to regular time series. Other Transformer methods convert sequences into the visual domain to leverage advanced vision backbones [3] or prioritize minimizing reconstruction error for masked input sequences during pretraining [21] or task-specific training [22]. Instead, STaRFormer emphasizes to maximize agreement between class-wise and batch-wise similarities in the latent space via contrastive learning (CL). This approach employs regional masking to manipulate key task-specific regions within an input sequence, introducing synthetic variations in statistical properties such as mean and variance (non-stationary) and sampling frequency (irregularly sampled). By incorporating this masking layer during the learning process of a downstream task, STaRFormer generates masked and unmasked latent representations of the same input sequence. Through a novel combination of self-supervised and supervised contrastive learning, we create robust task-informed latent embeddings, optimizing the balance between batch-wise and class-wise similarities. This technique is designed to enhance the model’s robustness to irregularities in time series while serving as an augmentation method to improve performance for regular sequential data tasks. In summary, our main **contributions** are:

- We propose STaRFormer, a highly effective approach boosting the performance of downstream tasks for diverse types of time series.
- We develop a novel semi-supervised CL approach for time series analysis, leveraging batch-wise and class-wise similarities by reconstructing latent representations from masked inputs.
- We design a novel Dynamic Attention-based Regional Masking (DAReM) scheme that identifies task-specific important regions of a sequence and forces the model to reconstruct the latent representation.
- We assess STaRFormer using a real-world dataset and 14 public datasets to validate its effectiveness compared to state-of-the-art methods, highlighting its versatility for various types of time series.

## 2 Related Work

**Non-stationary time series modeling** addresses the variability in statistical properties over time, such as changing means and covariances [23, 24]. Traditional models often fail to capture these dynamics. While most research has focused on forecasting, some efforts have been directed towards non-stationary time series classification. Recent advancements include adaptive Recurrent Neural Networks (RNNs) [25, 26], normalization-based approaches [27, 28], and non-stationary Transformers, which incorporate non-stationary factors to improve accuracy while addressing distribution shifts [29].

**Irregularly sampled time series modeling** addresses sequences with varying time intervals between observations. This challenges methods that assume regular sampling. A common solution is converting continuous time observations into fixed intervals [13, 15]. Several models have been proposed to capture dynamics between observations like GRU-D [16] and multi-directional RNN [30]. Attention-based models, including Transformers, [2, 21] and ATTAIN [31], incorporate attention mechanisms to handle time irregularity. Raindrop [20] uses graph neural networks to model irregular time series as graphs. Recently, ViTST [3] focused on time series in the visual modality by transforming sequences into visualized line graphs and leveraging pretrained Vision-Transformer backbones.

**Contrastive Learning** has proven effective in extracting high-quality, discriminative features [32]. CL operates as a self-supervised learning paradigm, learning representations by contrasting positive and negative pairs. The goal is to bring similar (positive) pairs closer and push dissimilar (negative) pairs apart, typically using contrastive losses like NT-Xent [32], InfoNCE [33], or triplet loss [34]. For sequential data, methods such as Time-CL (TCL) [35], Scalable Representation Learning (SRL or T-Loss) [36], and Temporal Neighborhood Coding (TNC) [37] use subsequence-based sampling,

assuming distant segments as negative pairs and neighboring segments as positive pairs. Other methods use instance-based sampling [38, 39], treating each sample individually. For a survey on CL, refer to Mohammadi Foumani et al. [40] and the references therein.

**Regular time series modeling for classification** involves analyzing sequential data collected over consistent time intervals to identify patterns and classify data. Baseline models include dimension-dependent dynamic time warping (DTWD) [41, 42] and symbolic representation models like WEASEL-MUSE, which use Symbolic Fourier Approximation (SFA) to capture local and global patterns [43]. Deep Learning (DL) stands powerful for time series classification by automatically extracting complex features. Unlike traditional methods that rely on handcrafted features, DL models such as RNN [44, 45], LSTM [1] and GRU [14], learn hierarchical representations directly from data. However, these models often struggle with capturing long term dependencies and spatiotemporal patterns. Convolutional Neural Networks (CNNs) have been effective in capturing local dependencies. Models like ROCKET [46] and MiniROCKET [47] have achieved remarkable results by learning features through diverse random convolutional kernels. Transformer-based approaches have recently gained attention due to their ability to capture long range dependencies in sequential data. Various Transformer-based models have been proposed for forecasting, classification, and anomaly detection [28, 48–52]. Initial approaches utilized a full encoder-decoder Transformer architecture for univariate time series forecasting [53], while TST [21] generalizes unsupervised representation learning for Transformer and time series, similarly to BERT’s Masked Language Modeling (MLM) [54]. TARNet, [22] addresses the issue of decoupling unsupervised pretraining from downstream tasks by using dynamic masking and reconstruction. Meanwhile, TrajFormer [55] introduces a Transformer architecture that generates continuous point embeddings to deal with irregularities of trajectories.

### 3 Approach

Let  $\mathcal{D} = \{(\mathbf{S}^{(i)}, y^{(i)}) \mid i = 1, \dots, M\}$  denote a time series dataset containing  $M$  samples. Each sequence,  $\mathbf{S}^{(i)} \in \mathbb{R}^N$  has  $N$  elements and is assigned to a label  $y^{(i)} \in \{1, \dots, C\}$ , where  $C$  is the number of classes. Each data point in the sequence can have an associated timestamp. Thus, the  $j$ -th data point in  $\mathbf{S}^{(i)}$  can be represented as  $\mathbf{s}_j^{(i)} = (x_j^{(i)}, t_j^{(i)}) \in \mathbb{R}^2$ . Therefore,  $\mathbf{S}^{(i)} = \{\mathbf{s}_j^{(i)} \mid j = 1, \dots, N\} \in \mathbb{R}^{N \times 2}$  is formed by concatenating all  $N$  elements. For multivariate time series, the dimensionality is not fixed to two, thus  $\mathbf{S}^{(i)} \in \mathbb{R}^{N \times D}$ , where  $N \in \mathbb{N}_{\neq 0}$  and  $D \in \mathbb{N}_{\geq 2}$ . A mini-batch, of size  $B$ , where  $B \ll M$  is defined as  $\mathbf{X} \subset \mathcal{D}$ ,  $\mathbf{X} \in \mathbb{R}^{N \times B \times D}$ .

**Problem 1.** Given a dataset  $\mathcal{D} = \{(\mathbf{S}^{(i)}, y^{(i)}) \mid i = 1, \dots, M\}$  where  $\mathbf{S}^{(i)} \in \mathbb{R}^{N \times D}$  is multivariate, predict the class  $y^{(i)} \in \{1, \dots, C\}$ , for each sequence  $\mathbf{S}^{(i)}$  in  $\mathcal{D}$ .

#### 3.1 Downstream Task

STaRFormer is based on an encoder-only Transformer architecture as shown in Fig. 1. STaRFormer consists of two ‘towers’ of  $N$  encoder blocks,  $f$ , that share a common set of model parameters. Without loss of generality, we consider classification as a downstream task, although STaRFormer can be extended to other tasks by adding different output heads, e.g., anomaly detection or regression. Instead of performing autoregressive predictions [22] or predictions based on the concatenation of the entire embedded representation [21], a special token is utilized for classification. This token effectively captures the dependencies between sequential elements via the encoder’s self-attention mechanism. A multilayer perceptron (MLP) performs the classification based on this token. The output of the MLP layer, i.e., the prediction  $\hat{y}^{(i)}$ , is passed through either the cross-entropy (CE) loss function for multi-class predictions,  $\mathcal{L}_{\text{CE}} = \sum_{i=1}^C y^{(i)} \log(\hat{y}^{(i)})$ , or the binary cross-entropy (BCE) loss for binary predictions,  $\mathcal{L}_{\text{CE}} = y^{(i)} \log(\hat{y}^{(i)}) + (1 - y^{(i)}) \log(1 - \hat{y}^{(i)})$ .

#### 3.2 Semi-Supervised Task Informed Representation Learning

##### 3.2.1 Dynamic Attention-based Regional Masking

Prior work has shown that task-specific importance of elements within a sequence varies w.r.t. their impact on downstream tasks [22, 56]. STaRFormer adopts this characteristic by dynamically masking regions around the features that the model deems important. This forces the model to learn changes in statistical properties and irregular sampling induced by the masking. Our rationale

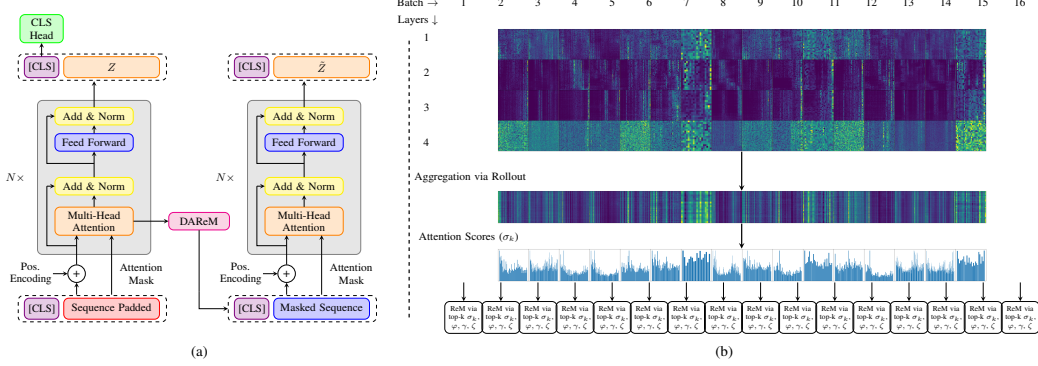


Figure 1: Architecture of STaRFormer; (a) High level architecture - the left tower performs the downstream task while the right tower performs reconstruction of the masked input sequence. (b) The Dynamic Attention-based Regional Masking (DAREm) methodology exemplified by a single batch from the DKT dataset with size 16 for an encoder with  $N = 4$  layers. ReM abbreviates regional mask.

is that reconstructing key sequential regions exaggerates non-stationary and irregular sampling characteristics. Compared to approaches that use random or no masking, this enables the model to generate more effective latent representations for the downstream task. During the computation of the multi-head attention, while executing the downstream task, STaRFormer dynamically collects the attention weights (left tower, Fig. 1). The attention weights gathered are denoted as  $\mathbf{A} \in \mathbb{R}^{L \times B \times N \times N}$ , where  $L, B, N$  represent the number of attention layers, mini-batch size, and number of elements in the sequences, respectively. We create a distinct masking scheme for each element in  $\mathbf{X}$ , resulting in  $B$  masks per  $\mathbf{X}$ . To aggregate the attention, STaRFormer employs a slightly modified attention rollout technique [57], rather than mere summation or aggregation. This approach enables a better consideration of the flow of information within the Transformer layers. The operation accounts for padded sequences by masking the attention if necessary, i.e.,

$$\tilde{\mathbf{A}} = \begin{cases} (\frac{1}{2}\mathbf{A}_{i,:,:,} \odot \mathbf{M} + \frac{1}{2}\mathbf{I}_N) \otimes \tilde{\mathbf{A}}_{i-1,:,:,} & \text{if } i > 0, \\ \mathbf{A}_{i,:,:,} \odot \mathbf{M} & \text{if } i = 0 \end{cases} \quad (1)$$

where  $\tilde{\mathbf{A}} \in \mathbb{R}^{B \times N \times N}$  represents the aggregated attention and  $\mathbf{M}$  the mask accounting for the padded input sequences. STaRFormer then computes the attention scores  $\sigma$  as in Chowdhury et al. [22], i.e.,

$$\sigma_{i,k'} = \frac{\sum_{j=1}^N \tilde{\mathbf{A}}_{i,j,k}}{\sum_{k=1}^N \sum_{j=1}^N \tilde{\mathbf{A}}_{i,j,k}}, \quad (2)$$

where  $\tilde{\mathbf{A}}_{i,j,k}$  is the attention weight assigned to  $s_k^{(i)}$  during the update of  $s_j^{(i)}$  in the transformers self-attention. A greater  $\sigma_{i,k'}$  value indicates a higher importance of the  $k$ -th element in  $\mathbf{S}^{(i)}$ .

The creation of the regional mask,  $g : \mathcal{D} \rightarrow \mathcal{R}$ , requires the hyperparameters:  $\varphi, \zeta, \gamma$ .  $\varphi$  determines the maximum amount of elements that are masked,  $\zeta$  determines the amount of sequential elements that are masked based on  $\sigma$ , and  $\gamma$  determines the bounds of the region to be masked.

### 3.2.2 Semi-supervised Contrastive Learning

Instead of concentrating on learning reconstructions of the representation during pretraining or a downstream task [54, 21, 22], STaRFormer enhances the latent space representation utilized by the model for its downstream task predictions. DAREm allows the creation of two correlated latent representations while training for a downstream task. As CL is known to extract high-quality, discriminative features [32–34, 39, 35, 36], STaRFormer facilitates CL to optimize the trade-off between these representations, see Fig. 2(a), by leveraging:

- **batch-wise positive pairs:** masked ( $\tilde{\mathbf{Z}}^{(i)}$ ) and unmasked ( $\mathbf{Z}^{(i)}$ ) embeddings of the same input sequence  $\mathbf{S}^{(i)}$
- **class-wise positive pairs:** masked ( $\tilde{\mathbf{Z}}^{(i)}$ ) and unmasked embeddings ( $\mathbf{Z}^{(i)}$ ) of the same class

Maximizing the alignment between batch-wise and class-wise latent representations aims to: strengthen the model’s robustness to perturbations; enhance generalization; reduce overfitting; and improve resilience to challenges like non-stationarity and irregular sampling. Based on the positive pairs, STaRFormer fuses two types of CL tasks: (i) **self-supervised** using batch-wise similarity and (ii) **supervised** using class-wise similarity. When sampling mini-batches during training, the latent variable becomes a three-dimensional tensor representation,  $\mathbf{Z}, \tilde{\mathbf{Z}} \in \mathbb{R}^{N \times B \times F}$ , where  $\mathbf{Z} = f(\mathbf{X})$ ,  $\tilde{\mathbf{Z}} = f(g(\varphi, \gamma, \zeta, \mathbf{X}))$  and  $F$  is the dimension of the latent embedding. To extract the similarity scores per sequential element in the batch (before computing the cosine similarity,  $\text{sim}(\mathbf{u}, \mathbf{v}) = \mathbf{u}^T \mathbf{v} / \|\mathbf{u}\| \|\mathbf{v}\|$ ), we compute the mean,  $\hat{\mathbf{Z}}_{i,j}$ , along the first dimension of the latent variables, thus  $\hat{\mathbf{Z}}_{i,j} = \frac{1}{N} \sum_{h=1}^N \mathbf{Z}_{h,i,j}$ . Elements at position  $i$  in the latent embedding originate from the same input sequence  $\mathbf{S}^{(i)}$ . Thus, given  $\hat{\mathbf{Z}}_{i,j} \in \mathbb{R}^{B \times F}$ , STaRFormer can form  $B$  positive and  $B(B-1)$  negative batch-wise pairs. By having  $C$  classes per  $\mathbf{X}$ , we obtain  $\sum_{c=1}^C n_c^2$  positive and  $\left(\sum_{c=1}^C n_c\right)^2 - \left(\sum_{c=1}^C n_c^2\right)$  negative class-wise pairs;  $n_c$  is the number of samples per class per  $\mathbf{X}$ . The batch-wise contrastive loss for a single positive batch-wise sample is:

$$l_{\text{bw}}^{(i)} = -\log \frac{\exp\left(\text{sim}\left(\hat{\mathbf{z}}^{(i)}, \hat{\mathbf{z}}^{(i)}\right) / \tau\right)}{\sum_{k=1}^B \mathbb{I}_{[k \neq i]} \exp\left(\text{sim}\left(\hat{\mathbf{z}}^{(i)}, \hat{\mathbf{z}}^{(k)}\right) / \tau\right)} \quad (3)$$

and the class-wise contrastive loss for a single positive class-wise sample is formulated as:

$$l_{\text{cw}}^{(i)} = -\log \frac{\sum_{j=1}^B \mathbb{I}_{[c_j = c_i]} \exp\left(\text{sim}\left(\hat{\mathbf{z}}^{(i)}, \hat{\mathbf{z}}^{(j)}\right) / \tau\right)}{\sum_{k=1}^B \mathbb{I}_{[c_k \neq c_i]} \exp\left(\text{sim}\left(\hat{\mathbf{z}}^{(i)}, \hat{\mathbf{z}}^{(k)}\right) / \tau\right)} \quad (4)$$

The indicator function differs in the two cases:  $\mathbb{I}_{[k \neq i]}$  for batch-wise, which is 1 iff  $k \neq i$ ,  $\mathbb{I}_{[c_k \neq c_i]}$  for class-wise, which is 1 if the class of  $i$  is different from class of  $k$ , and vice versa for  $\mathbb{I}_{[c_k = c_i]}$ . The fused contrastive loss weighs batch-wise and class-wise contrastive losses:

$$\mathcal{L}_{\text{STaR-CL}} = \lambda_{\text{fuse-CL}} \mathcal{L}_{\text{bw}} + (1 - \lambda_{\text{fuse-CL}}) \mathcal{L}_{\text{cw}}, \quad (5)$$

where  $\mathcal{L}_{\text{bw}} = \frac{1}{B} \sum_{i=1}^B l_{\text{bw}}^{(i)}$  and  $\mathcal{L}_{\text{cw}} = \frac{1}{B} \sum_{i=1}^B l_{\text{cw}}^{(i)}$ . STaRFormer’s loss is a weighted sum of  $\mathcal{L}_{\text{CE}}$  and the fused contrastive loss,  $\mathcal{L}_{\text{STaR-CL}}$ :

$$\mathcal{L}_{\text{STaRFormer}} = \mathcal{L}_{\text{CE}} + \lambda_{\text{CL}} \mathcal{L}_{\text{STaR-CL}}, \quad (6)$$

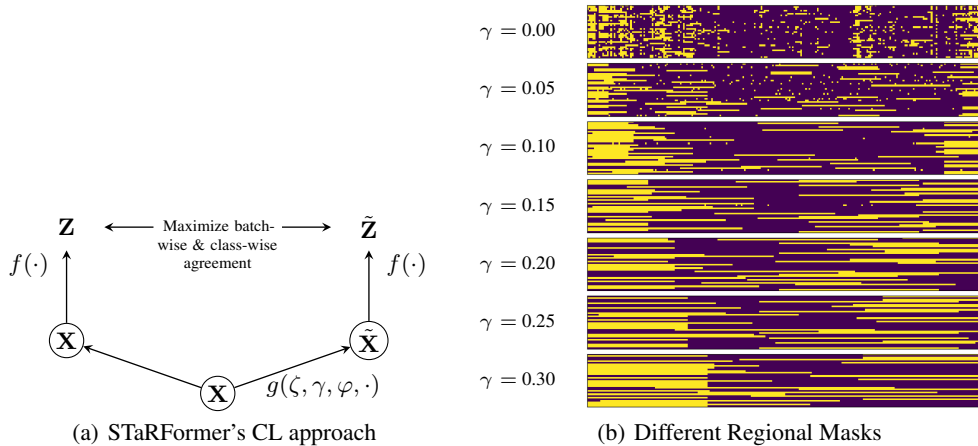


Figure 2: Components of the STaRFormer’s semi-supervised CL approach, where (a) displays the CL schematically, where the masking,  $g$ , generates two correlated views. The encoder,  $f$ , is trained to maximize the trade-off between batch- and class-wise agreement of the latent embeddings  $\mathbf{Z}$  and  $\tilde{\mathbf{Z}}$  while training for a downstream task. (b) displays seven different regional masks for the same batch, with sequences aligned horizontally and stacked vertically (per  $\mathbf{X}$ ). The masked regions in DAREM are defined by different values of  $\gamma$ , with  $\varphi \approx 0.2$  and  $\zeta = 0.3$  held constant and depicted in yellow.

where  $\lambda_{CL}$  is a tunable hyperparameter and  $\lambda_{fuse-CL} = 0.5$  to weigh batch- and class-wise similarities equally.

## 4 Experiments

We conduct experiments on a range of datasets across different time series types including non-stationary, irregularly sampled, spatiotemporal and regular time series from various domains. For each public dataset, STaRFormer compares against respective state-of-the-art methods to evaluate its effectiveness. Moreover, we conduct ablation studies in Section 4.2 to verify the performance gains of STaRFormer’s masking and CL paradigms. For all methods, the accuracy on the test sets is reported. For DKT and Geolife (GL) [70] datasets, the  $F_{0.5}$ -score is additionally reported. For Physical Activity Monitoring (PAM) [71], precision, recall, and  $F_1$ -score are reported. All models were trained on 16GB Tesla V100-SXM2s.

### 4.1 Main Results

#### 4.1.1 Spatiotemporal Time Series

We use the GL dataset [70] to evaluate STaRFormer on spatiotemporal sequential data, as it resembles the data type found in the DKT dataset. To determine if the dataset exhibits non-stationary characteristics, we conduct KPSS and ADF tests [72, 73]. Due to real-world recorded GPS data, i.e., subject to environmental influences, we expected some degree of non-stationary time series [10]. Our analysis revealed that 93% of the data used for training and validation is non-stationary. STaRFormer outperforms all previous methodologies, including classical models such as SVM, LSTM, ST-GRU [17], and Transformer architectures [55] as shown in Table 1, improving the current state-of-the-art by 1.9 percentage points. For comparability with literature, we too report only the top score in Table 1. Nonetheless, we compute STaRFormer across five different seeds, altering the dataset samples used for training, testing and the model’s deterministics.

#### 4.1.2 Irregularly Sampled Time Series Data

We compare STaRFormer against state-of-the-art methods designed for irregularly sampled time series on the PAM dataset [71] including Transformer [2], GRU-D [16], SeFT [18], mTAND [19], IP-Net [74], Raindrop [20], and ViTST [3]. To ensure fairness, the performance metrics are averaged over five consistent data splits. Across all models, STaRFormer achieves state-of-the-art results, surpassing all previously mentioned models, improving ViTST by 1.8, 1.1, 1.5 and 0.9 percentage points

Table 1: Classification results for the non-stationary, spatiotemporal time series. Models marked with \*\* are from Liu et al. [17] and ++ from Liang et al. [55].

	RNN <sup>++</sup>	Time-LSTM <sup>**</sup>	TrajFormer <sup>++</sup>	SVM <sup>**</sup>	Random Forest <sup>**</sup>	CNN <sup>**</sup>	LSTM <sup>**</sup>	GRU <sup>**</sup>	ST-GRU <sup>**</sup>	STaRFormer
Accuracy	0.643	0.839	0.855	0.861	0.869	0.871	0.884	0.898	<u>0.913</u>	<b>0.932</b>

Table 2: Classification results for PAM (in %).

	Accuracy	Precision	Recall	$F_1$ -Score
Transformer <sup>†</sup>	83.5 ± 1.5	84.8 ± 1.5	86.0 ± 1.2	85.0 ± 1.3
Trans-mean <sup>†</sup>	83.7 ± 2.3	84.9 ± 2.6	86.4 ± 2.1	85.1 ± 2.4
GRU-D <sup>†</sup>	83.9 ± 1.6	84.6 ± 1.2	85.2 ± 1.6	84.8 ± 1.2
SeFT <sup>†</sup>	67.1 ± 2.2	70.0 ± 2.4	68.2 ± 1.5	68.5 ± 1.8
mTAND <sup>†</sup>	74.6 ± 4.3	74.3 ± 4.0	79.5 ± 2.8	76.8 ± 3.4
IP-Net <sup>†</sup>	74.3 ± 3.8	75.6 ± 2.1	77.9 ± 2.2	76.6 ± 2.8
Raindrop <sup>†</sup>	88.5 ± 1.5	89.9 ± 1.5	89.9 ± 0.6	89.8 ± 1.0
ViTST <sup>†</sup>	<u>95.8 ± 1.3</u>	<u>96.2 ± 1.3</u>	<u>96.1 ± 1.1</u>	<u>96.5 ± 1.2</u>
<b>STaRFormer</b>	<b>97.6 ± 0.9</b>	<b>97.3 ± 0.4</b>	<b>97.6 ± 0.3</b>	<b>97.4 ± 0.3</b>

Table 3: Classification results for DKT.

	Accuracy	$F_{0.5}$
RNN	0.754 ± 0.010	0.754 ± 0.010
LSTM	0.847 ± 0.004	0.847 ± 0.003
GRU	0.849 ± 0.003	0.849 ± 0.003
<b>STaRFormer</b>	<b>0.852 ± 0.003</b>	<b>0.852 ± 0.003</b>

Table 4: Classification results for the UCR-UEA datasets.

	DTWD <sup>*</sup>	DTWI <sup>*</sup>	LSTM <sup>+</sup>	Rocket <sup>*</sup>	Mini-Rocket <sup>*</sup>	TST <sup>†</sup>	TST (pretrained) <sup>+</sup>	TARNet <sup>*</sup>	ViTST <sup>†</sup>	STaRFormer
EW [58]	0.618	-	0.650	0.790	-	-	0.420	<b>0.878</b>	0.850	
EC [59]	0.323	0.304	0.323	<u>0.450</u>	0.430	0.337	0.326	0.323	<b>0.456</b>	
FD [60]	0.529	0.577	0.638	0.612	0.681	0.681	<u>0.689</u>	0.641	<b>0.697</b>	
HW [61]	0.286	0.316	0.152	<b>0.596</b>	0.520	0.305	0.359	0.281	0.373	
HB [62]	0.717	0.658	0.722	0.741	0.771	<u>0.776</u>	0.776	<b>0.780</b>	0.766	
JV [63]	0.949	0.959	0.797	0.978	0.986	<u>0.994</u>	<b>0.997</b>	0.992	0.946	
PD [64]	0.977	0.939	-	<u>0.981</u>	0.967	-	-	0.976	-	
PS [65]	0.711	0.734	0.399	0.832	0.809	0.919	0.896	<u>0.936</u>	0.913	
SCP1 [66]	0.775	0.765	0.689	0.867	0.915	<b>0.925</b>	<u>0.922</u>	0.816	0.898	
SCP2 [67]	0.539	0.533	0.466	0.555	0.506	0.589	0.604	<u>0.622</u>	0.561	
SAD [68]	0.963	0.959	0.319	0.997	0.963	<u>0.993</u>	<b>0.998</b>	0.985	0.985	
UW [69]	0.903	0.868	0.412	<b>0.931</b>	0.785	0.903	<u>0.913</u>	0.878	0.862	
Average Accuracy 8	0.735	0.723	0.516	0.794	0.771	<u>0.805</u>	0.804	0.792	0.798	
Rank 8	8	9	10	5	7	<u>2</u>	3	6	4	
Average Rank 8	7.3	8.5	9.4	4.5	6.0	<u>2.9</u>	<b>2.8</b>	4.1	5.4	
Num. of Top Scores	0	0	0	2	0	1	2	1	2	
STaRFormer 1-v-1	11	10	10	8	9	5	6	10	8	
Dataset Count	12	10	10	12	12	10	10	12	10	

The model results marked with \* are taken from the Chowdhury et al. [22], + from Zerveas et al. [21], † from Li et al. [3], \*\* from Liu et al. [17] and ++ from Liang et al. [55].

for accuracy, precision, recall and F1-score, respectively (see Table 2). Furthermore, STaRFormer yields predictions with significantly smaller standard deviations across all metrics, indicating greater consistency, reliability, and reduced performance variability compared to other methods.

### 4.1.3 Non-Stationary, Spatiotemporal and Irregularly Sampled Data

We examine STaRFormer’s performance on the DKT dataset consisting of a mixture of non-stationary, spatiotemporal and irregularly sampled time series data. The DKT dataset includes 559,709 labeled anonymized customer trajectories recorded over three months using DKs and UWB for high-precision localization near vehicles. We implement extensively hyperparameter tuned RNN, LSTM and GRU networks as baseline models. The scores reported in Table 3 are averaged across five seeds. STaRFormer improves accuracy by and  $F_{0.5}$ -score by **9.9**, **0.5** and **0.3** percentage points compared to the RNN, LSTM and GRU, respectively.

### 4.1.4 Regular Time Series

We use 12 datasets from the UCR, UEA, and UCI ML repositories (UCR-UEA) [75–78] to compare STaRFormer against DTWD and DTWI [42], LSTM, Rocket [46], Mini-Rocket [47] and Transformer-based approaches, i.e., TST, TST pretrained [21], TARNet [22], ViTST [3]. The datasets in Table 4 cover a variety of domains, sensor types, sampling frequencies, numbers of training and testing samples, time series lengths, feature counts, and target classes for comprehensive evaluation. The results are presented in Table 4. Our analysis focuses on 8 out of 12 datasets for which all models report performance metrics (accuracy) to ensure a meaningful comparison. On UCR-UEA-8, STaRFormer achieves the highest accuracy (**0.816**) with **1.1** improvement in percentage points. On the FD, PD, PS, and SCP2 datasets, STaRFormer scores the highest among all models. Although TST’s average rank is slightly higher than STaRFormer, this metric should be interpreted cautiously, as accuracy differences are minimal ( $< 0.1$ ). Therefore, we conduct direct model-vs-model comparisons. STaRFormer outperforms TST and TST (pretrained) in 5/10 and 6/10 datasets respectively, TARNet in 10/12 datasets, and ViTST in 8/10 datasets. In the head-to-head comparison between STaRFormer and TST, STaRFormer beats TST by an average margin of 0.042 while TST conversely outperforms STaRFormer by only 0.006, indicating STaRFormer’s ‘wins’ are more substantial than its ‘losses’. Overall, on average, STaRFormer outperforms all models across the benchmark.

## 4.2 What contributes to STaRFormer performance?

### 4.2.1 Approach

STaRFormer matches or outperforms state-of-the-art on non-stationary, irregularly sampled, spatiotemporal and regular sequential data. To showcase the performance gains achieved by DAREM paired with semi-supervised CL in STaRFormer, we train ablations: an encoder-only Transformer (Base), left tower in Fig. 1 and STaRFormer with RM, and compare to STaRFormer (with DAREM).

Table 5: STaRFormer ablation study results.

	Base	STaRFormer-RM	STaRFormer
DKT	0.851 ± 0.002	0.845 ± 0.001	<b>0.852</b> ± 0.003
GL	0.881 ± 0.012	0.894 ± 0.014	<b>0.908</b> ± 0.013
PAM	0.964 ± 0.013	0.964 ± 0.011	<b>0.976</b> ± 0.009
EW	0.371	<b>0.402</b>	0.393
EC	0.752	0.799	<b>0.850</b>
FD	0.687	0.673	<b>0.697</b>
HW	0.336	0.327	<b>0.373</b>
HB	<b>0.786</b>	0.772	0.772
JV	<b>0.990</b>	0.982	<b>0.990</b>
PD	0.982	0.980	<b>0.983</b>
PS	0.909	0.922	<b>0.943</b>
SCP1	0.906	0.891	<b>0.913</b>
SCP2	0.630	0.620	<b>0.635</b>
SAD	<b>0.990</b>	0.983	0.989
UW	0.881	0.838	<b>0.894</b>
Avg. Acc.	0.794	0.793	<b>0.811</b>
Rank	2	3	<b>1</b>
Avg Rank	2.2	2.5	<b>1.2</b>
Top Scores	2	1	<b>12</b>
<b>I-v-1</b>			
Base	-	10	2
RM	5	-	1
STaRFormer	12	13	-

Table 6: Ablation study results of the semi-supervised contrastive learning paradigm.

CL Method	DKT ( $\lambda_{CL} \approx 0.796$ )		GL ( $\lambda_{CL} \approx 0.773$ )		PAM ( $\lambda_{CL} \approx 0.567$ )			
	Acc	$F_{0.5}$	Acc	$F_{0.5}$	Acc	Precision	Recall	$F_1$
semi-supervised	<b>85.2</b> ± 0.3	<b>85.2</b> ± 0.3	90.4 ± 1.6	88.3 ± 1.9	<b>97.6</b> ± 0.9	97.3 ± 0.4	<b>97.6</b> ± 0.3	<b>97.4</b> ± 0.3
w/o self-supervised	84.8 ± 0.2	84.8 ± 0.2	90.0 ± 1.4	87.7 ± 1.5	96.3 ± 1.9	97.0 ± 0.7	96.9 ± 0.5	97.3 ± 0.8
w/o supervised	84.8 ± 0.1	84.7 ± 0.2	89.5 ± 1.6	87.7 ± 1.4	96.5 ± 1.6	<b>97.5</b> ± 0.3	<b>97.4</b> ± 0.5	<b>97.4</b> ± 0.3
semi-supervised, $\lambda_{CL} = 0.1$	84.8 ± 0.1	84.6 ± 0.4	90.0 ± 1.8	87.9 ± 2.1	96.8 ± 1.2	96.9 ± 0.2	97.3 ± 0.3	97.1 ± 0.1
semi-supervised, $\lambda_{CL} = 1$	<b>85.1</b> ± 0.2	<b>85.1</b> ± 0.2	90.2 ± 1.3	88.0 ± 1.5	<b>97.2</b> ± 0.7	97.4 ± 0.3	97.2 ± 0.7	97.3 ± 0.4
semi-supervised, $\lambda_{CL} = 5$	84.9 ± 0.2	84.9 ± 0.2	<b>90.8</b> ± 1.3	<b>88.7</b> ± 1.6	96.7 ± 2.3	<b>97.5</b> ± 1.2	97.0 ± 1.7	97.2 ± 1.5
semi-supervised, $\lambda_{CL} = 10$	84.6 ± 0.3	84.6 ± 0.3	<b>90.6</b> ± 1.0	<b>88.5</b> ± 1.3	97.0 ± 1.6	<b>97.7</b> ± 0.7	<b>97.6</b> ± 0.7	<b>97.6</b> ± 0.7

Table 7: One-at-a-time analysis examining the effect of masking various region sizes iteration of various  $\gamma$  while keeping  $\varphi$  and  $\zeta$  are kept constant.

#	$\gamma$	DKT ( $\varphi \approx 0.427, \zeta = 0.2$ )		GL ( $\varphi \approx 0.472, \zeta = 0.3$ )		PAM ( $\varphi \approx 0.207, \zeta = 0.3$ )			
		Accuracy	$F_{0.5}$	Accuracy	$F_{0.5}$	Accuracy	Precision	Recall	$F_1$
1	0.00	85.0 ± 0.2	85.0 ± 0.2	89.8 ± 1.9	87.9 ± 1.8	97.0 ± 0.7	<b>97.4</b> ± 0.2	97.3 ± 0.6	97.3 ± 0.3
2	0.05	85.0 ± 0.3	84.8 ± 0.3	<b>90.4</b> ± 1.6	<b>88.3</b> ± 1.9	94.9 ± 2.5	96.5 ± 0.6	96.6 ± 0.5	96.5 ± 0.4
3	0.10	84.9 ± 0.3	84.9 ± 0.2	<b>90.3</b> ± 1.2	88.2 ± 1.3	<b>97.6</b> ± 0.9	97.3 ± 0.4	<b>97.6</b> ± 0.3	<b>97.4</b> ± 0.3
4	0.15	85.0 ± 0.2	85.0 ± 0.2	<b>90.3</b> ± 1.5	88.2 ± 1.7	<b>97.1</b> ± 1.1	<b>97.5</b> ± 0.6	<b>97.5</b> ± 1.0	<b>97.5</b> ± 0.8
5	0.20	<b>85.1</b> ± 0.1	<b>85.1</b> ± 0.1	90.1 ± 1.1	87.9 ± 1.0	96.2 ± 0.8	96.7 ± 0.5	96.6 ± 0.6	96.6 ± 0.4
6	0.25	<b>85.2</b> ± 0.3	<b>85.2</b> ± 0.3	90.1 ± 1.6	<b>88.4</b> ± 1.4	96.3 ± 0.9	96.9 ± 0.7	96.5 ± 0.6	96.7 ± 0.5
7	0.30	85.0 ± 0.1	85.0 ± 0.1	<b>90.3</b> ± 1.3	88.2 ± 1.4	96.3 ± 0.9	96.7 ± 0.5	96.4 ± 0.5	96.5 ± 0.4

Table 5 demonstrates that Base ablation delivers a competitive performance achieving highest scores in 2 datasets. STaRFormer outperforms STaRFormer-RM in 13 out of 15 datasets, while STaRFormer-RM outperforms STaRFormer only in 1 dataset. This verifies that DAREM significantly enhances the robustness of predictions across a variety of time series modeling tasks compared to RM. STaRFormer (0.811) surpasses the two ablation variants (Base & STaRFormer-RM) by 1.7 and 1.8 percentage points respectively, achieving the highest number of top scores (12) and best average rank (1.2). Furthermore, STaRFormer performs significantly better on UCR-UEA datasets with only a few samples, suggesting its capacity as an augmentation technique especially for lower data regimes. The ablation study supports the competitive performance and validates the efficacy of DAREM with semi-supervised CL in STaRFormer.

#### 4.2.2 Impact of Semi-Supervised CL

Next, we examine the impact of the different components of the semi-supervised CL in STaRFormer. All parameters are fixed and only the respective components are removed from the loss. For DKT and GL, we rerun the best configuration for five seeds. For PAM, we use the same five splits as previously. Furthermore, we study the impact of combining CL and CE via  $\lambda_{CL}$ , Eq. (6). The results in Table 6 show the advantages of maximizing agreement between both batch-wise and class-wise representations in CL. Across all datasets, the downstream task performance (accuracy) declined by 0.4 to 1.1 percentage points when these representations were not fused in the CL approach. There is no consistent trend favoring one representation over the other; e.g., in GL, supervised CL outperformed self-supervised CL, while the opposite holds for PAM. In DKT, both methods yield comparable results. We further examined the influence of  $\mathcal{L}_{STaR-CL}$  on the overall loss by adjusting  $\lambda_{CL}$ . The scale difference between  $\mathcal{L}_{CE}$  and  $\mathcal{L}_{STaR-CL}$  is approximately a factor of 10 across all datasets. Consequently, values of  $\lambda_{CL} > 0.1$  assign greater weight to  $\mathcal{L}_{STaR-CL}$ , thus increasing its impact on the overall loss and the model updates during backpropagation. Our results indicate that higher values of  $\lambda_{CL}$  lead to improved performance, with all top scores achieved at  $\lambda_{CL} > 0.1$  (in some cases, large weights of 5 and 10 yielded best results). The findings support our approach. Prioritizing the maximization of agreement between task-aware batch-wise and class-wise latent representations via CL during training improves classification performance compared to focusing solely on the classification task.

#### 4.2.3 Impact of Regional Masking

STaRFormer creates regional masks based on the importance of sequential elements in a sequence allowing semi-supervised CL. In Section 3.2.1, we introduced  $\varphi$ ,  $\zeta$  and  $\gamma$  to create the masks, where  $\gamma$  defines the size of a region to be masked. To examine the impact and benefit of masking regions, we perform an one-at-a-time analysis (OAT), where we iteratively change  $\gamma$  while keeping all other parameters fixed. We expect better performance when using larger masking regions around the top- $k$ , i.e.,  $\gamma > 0$ , compared to only masking the top- $k$  important sequential elements, i.e.,  $\gamma = 0$ . However, one would expect that if the masked regions are too large, it would harm the performance as the model would reconstruct from a base sequence with little information. Fig. 2(b) shows the influence of  $\gamma$  on the creation of masks in STaRFormer. Table 7 reports the results of this ablation study. The observed trend indicates that on a macro scale, masking larger regions enhances the performance of STaRFormer. Masking regions larger than 10% of the global sequence length around the selected elements achieves top scores for 7 out of 8 metrics in Table 7. For instance, the accuracies for DKT, GL, and PAM were 0.850, 0.898, and 0.970 with  $\gamma = 0$ , compared to 0.852, 0.908, and 0.976 for optimal configurations of  $\gamma$ , 0.25, 0.05, and 0.1, respectively. On a micro scale, performance peaks were observed at optimal configurations with the best performance for DKT at  $\gamma = 0.25$ . For GL and PAM, the performance peaks were found for smaller region masks. Further increasing or decreasing the masked regions gradually deteriorated the results, supporting our initial hypothesis. These findings emphasize the significance of masking regions rather than individual sequential elements. The results underscore the necessity of precisely calibrating masking parameters to optimize the model’s performance.

#### 4.2.4 Latent Space Analysis

To evaluate the hypothesis that enhancing the latent embedding space improves prediction performance, we analyzed t-Distributed Stochastic Neighbor Embedding (t-SNE) visualizations [79] for datasets: DKT, Fig. 3(a) and 3(b), PAM, Fig. 3(c) and 3(d), GL, Fig. 3(e) and 3(f), and PS, Fig. 3(g)



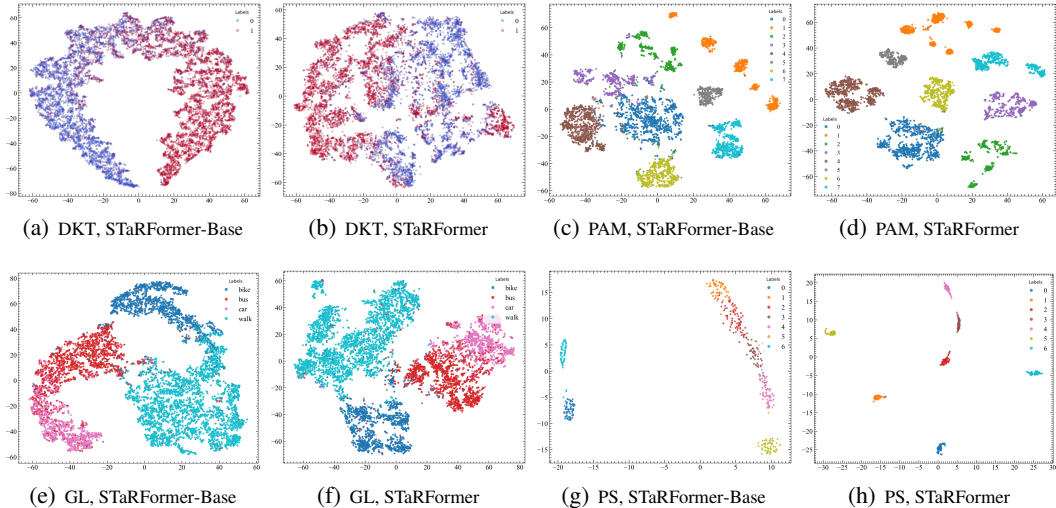


Figure 3: Visualizations of model latent spaces using t-SNE; (a) and (b) are representations of the DKT dataset, (c) and (d) of the PAM dataset, (e) and (f) of the GL dataset and (g) and (h) of the PS dataset (UCR-UEA). All t-SNE plots were plotted with perplexity 50.

and 3(h). On these datasets, STaRFormer outperforms the Base ablation. Each dataset is represented by t-SNE plots comparing the latent spaces of Base and STaRFormer. The t-SNE plots reveal that while Base achieves class separation, STaRFormer consistently produces distinct and well-separated clusters for each class across all datasets (classes are color-coded). For instance, in DKT, the latent embeddings for both models show overlap between class clusters. However, STaRFormer is able to more distinctly separate clusters between the classes, whereas Base has one significant area of overlap. This trend is amplified by the observations in PAM and GL, where STaRFormer displays more distinct clusters with minimal overlap compared to Base. In GL, clusters for ‘walk’ and ‘bike’ as well as ‘car’ and ‘bus’ are distinctly separated, though distinguishing between ‘car’ and ‘bus’ remains challenging due to similar traveling speeds and trajectories. In PS, we obtain the most pronounced difference with Base producing scattered clusters with significant overlap, while STaRFormer achieves distinctly separated clusters. These results align with the test accuracy reported in Table 5, where the accuracy difference between the Base and STaRFormer is most significant on PS. In summary, for datasets with similar test accuracies, the clusters from both models appear more similar. STaRFormer creates better separated latent spaces, indicating a stronger capability for class separation, which considering the improved test accuracy, leads to improved classification performance compared to the Base ablation. For datasets where our CL approach is very effective, e.g., PS, the improvement through our approach is clearly visualized in the t-SNE visualizations.

## 5 Discussion and Conclusion

We introduce an innovative semi-supervised CL technique that exploits both batch-wise (self-supervised) and class-wise (supervised) similarities within latent embeddings produced by STaRFormer. These embeddings are generated using our novel Dynamic Attention-based Regional Masking scheme. By integrating this scheme with CL, we achieve improved task-specific representations for predictions on downstream tasks. Comprehensive experiments demonstrate that STaRFormer either surpasses or is on par with state-of-the-art techniques for spatiotemporal and irregularly sampled time series. It also shows promising capabilities on regular and non-stationary time series. We verify this performance on benchmark datasets and real world data from our industrial partner. One noted limitation is the computational cost associated with the attention weights-based masking approach, particularly for long sequences. The quadratic complexity,  $\mathcal{O}(N^2)$ , of the attention mechanism might be expensive. Future work could explore more efficient attention mechanisms, such as flash attention, to enhance the scalability of STaRFormer for long sequences.

## References

- [1] Sepp Hochreiter and Jürgen Schmidhuber. Long Short-Term Memory. *Neural Computation*, 9(8):1735–1780, November 1997. ISSN 0899-7667. doi: 10.1162/neco.1997.9.8.1735. URL <https://doi.org/10.1162/neco.1997.9.8.1735>.
- [2] Ashish Vaswani, Noam Shazeer, Niki Parmar, Jakob Uszkoreit, Llion Jones, Aidan N Gomez, Łukasz Kaiser, and Illia Polosukhin. Attention is All you Need. In *Advances in Neural Information Processing Systems*, volume 30. Curran Associates, Inc., 2017. URL [https://proceedings.neurips.cc/paper\\_files/paper/2017/hash/3f5ee243547dee91fbd053c1c4a845aa-Abstract.html](https://proceedings.neurips.cc/paper_files/paper/2017/hash/3f5ee243547dee91fbd053c1c4a845aa-Abstract.html).
- [3] Zekun Li, Shiyang Li, and Xifeng Yan. Time Series as Images: Vision Transformer for Irregularly Sampled Time Series. *Advances in Neural Information Processing Systems*, 36: 49187–49204, December 2023. URL [attent](https://arxiv.org/abs/2310.12345).
- [4] Apple. Explore UWB-based car keys - WWDC21 - Videos, June 2021. URL <https://developer.apple.com/videos/play/wwdc2021/10084/>.
- [5] BMW. BMW announces support for Digital Key for iPhone. A secure and easy way to use iPhone as a car key to lock, unlock, drive, and share keys with friends., June 2020. URL <https://www.press.bmwgroup.com/global/article/detail/T0309827EN/bmw-announces-support-for-digital-key-for-iphone-a-secure-and-easy-way-to-use-iphone-as-a-car-key-to-lock-unlock-drive-and-share-keys-with-friends?language=en>.
- [6] BMW. What’s the deal with Ultra Wideband technology and what will it do for your car?, November 2021. URL <https://www.bmw.com/en/innovation/bmw-digital-key-plus-ultra-wideband.html>.
- [7] Mercedes-Benz. UWB, BLE Digital Car Key - E Klasse, April 2023. URL <https://media.mercedes-benz.com/press-kit/2b41d0bb-f447-4d97-bfde-c10339232424/article/ca92e61f-252f-408d-be80-a7d659909c72>.
- [8] Samsung. Samsung Wallet Adds Digital Key for Select Audi Vehicles, November 2024. URL <https://news.samsung.com/global/samsung-wallet-adds-digital-key-for-select-audi-vehicles>.
- [9] CCC. Digital Key Release 3, 2024. URL <https://carconnectivity.org/digital-key-release-3-0-specification-download/>. Version 1.1.3.
- [10] Luke Birmingham and Ickjai Lee. A probabilistic stop and move classifier for noisy GPS trajectories. *Data Min. Knowl. Discov.*, 32(6):1634–1662, November 2018. ISSN 1384-5810. doi: 10.1007/s10618-018-0568-8. URL <https://doi.org/10.1007/s10618-018-0568-8>.
- [11] M.A. Hearst, S.T. Dumais, E. Osuna, J. Platt, and B. Scholkopf. Support vector machines. *IEEE Intelligent Systems and their Applications*, 13(4):18–28, July 1998. ISSN 2374-9423. doi: 10.1109/5254.708428. URL <https://ieeexplore.ieee.org/document/708428?arnumber=708428>. Conference Name: IEEE Intelligent Systems and their Applications.
- [12] Leo Breiman. Random Forests. *Machine Learning*, 45(1):5–32, October 2001. ISSN 1573-0565. doi: 10.1023/A:1010933404324. URL <https://doi.org/10.1023/A:1010933404324>.
- [13] Benjamin M. Marlin, David C. Kale, Robinder G. Khemani, and Randall C. Wetzel. Unsupervised pattern discovery in electronic health care data using probabilistic clustering models. In *Proceedings of the 2nd ACM SIGHIT International Health Informatics Symposium, IHI ’12*, pages 389–398, New York, NY, USA, January 2012. Association for Computing Machinery. ISBN 978-1-4503-0781-9. doi: 10.1145/2110363.2110408. URL <https://doi.org/10.1145/2110363.2110408>.

- [14] Kyunghyun Cho, Bart van Merriënboer, Caglar Gulcehre, Dzmitry Bahdanau, Fethi Bougares, Holger Schwenk, and Yoshua Bengio. Learning Phrase Representations using RNN Encoder–Decoder for Statistical Machine Translation. In Alessandro Moschitti, Bo Pang, and Walter Daelemans, editors, *Proceedings of the 2014 Conference on Empirical Methods in Natural Language Processing (EMNLP)*, pages 1724–1734, Doha, Qatar, October 2014. Association for Computational Linguistics. doi: 10.3115/v1/D14-1179. URL <https://aclanthology.org/D14-1179>.
- [15] Zachary C. Lipton, David Kale, and Randall Wetzel. Directly Modeling Missing Data in Sequences with RNNs: Improved Classification of Clinical Time Series. In *Proceedings of the 1st Machine Learning for Healthcare Conference*, pages 253–270. PMLR, December 2016. URL <https://proceedings.mlr.press/v56/Lipton16.html>. ISSN: 1938-7228.
- [16] Zhengping Che, Sanjay Purushotham, Kyunghyun Cho, David Sontag, and Yan Liu. Recurrent Neural Networks for Multivariate Time Series with Missing Values. *Scientific Reports*, 8(1): 6085, April 2018. ISSN 2045-2322. doi: 10.1038/s41598-018-24271-9. URL <https://www.nature.com/articles/s41598-018-24271-9>. Publisher: Nature Publishing Group.
- [17] Hongbin Liu, Hao Wu, Weiwei Sun, and Ickjai Lee. Spatio-Temporal GRU for Trajectory Classification. In *2019 IEEE International Conference on Data Mining (ICDM)*, pages 1228–1233, November 2019. doi: 10.1109/ICDM.2019.00152. URL <https://ieeexplore.ieee.org/document/8970798/?arnumber=8970798>. ISSN: 2374-8486.
- [18] Max Horn, Michael Moor, Christian Bock, Bastian Rieck, and Karsten Borgwardt. Set Functions for Time Series. In *Proceedings of the 37th International Conference on Machine Learning*, pages 4353–4363. PMLR, November 2020. URL <https://proceedings.mlr.press/v119/horn20a.html>. ISSN: 2640-3498.
- [19] Satya Narayan Shukla and Benjamin Marlin. Multi-Time Attention Networks for Irregularly Sampled Time Series. October 2020. URL [https://openreview.net/forum?id=4c0J6lwQ4\\_](https://openreview.net/forum?id=4c0J6lwQ4_).
- [20] Xiang Zhang, Marko Zeman, Theodoros Tsiligkaridis, and Marinka Zitnik. Graph-Guided Network for Irregularly Sampled Multivariate Time Series. October 2021. URL <https://openreview.net/forum?id=Kwm8I7dU-15>.
- [21] George Zerveas, Srideepika Jayaraman, Dhaval Patel, Anuradha Bhamidipaty, and Carsten Eickhoff. A Transformer-based Framework for Multivariate Time Series Representation Learning. In *Proceedings of the 27th ACM SIGKDD Conference on Knowledge Discovery & Data Mining, KDD '21*, pages 2114–2124, New York, NY, USA, August 2021. Association for Computing Machinery. ISBN 978-1-4503-8332-5. doi: 10.1145/3447548.3467401. URL <https://dl.acm.org/doi/10.1145/3447548.3467401>.
- [22] Ranak Roy Chowdhury, Xiyuan Zhang, Jingbo Shang, Rajesh K. Gupta, and Dezhi Hong. TARNet: Task-Aware Reconstruction for Time-Series Transformer. In *Proceedings of the 28th ACM SIGKDD Conference on Knowledge Discovery and Data Mining*, pages 212–220, Washington DC USA, August 2022. ACM. ISBN 978-1-4503-9385-0. doi: 10.1145/3534678.3539329. URL <https://dl.acm.org/doi/10.1145/3534678.3539329>.
- [23] Christopher M. Bishop. *Pattern recognition and machine learning*. Information science and statistics. Springer, New York, 2006. ISBN 978-0-387-31073-2.
- [24] Rebecca Salles, Kele Belloze, Fabio Porto, Pedro H. Gonzalez, and Eduardo Ogasawara. Nonstationary time series transformation methods: An experimental review. *Knowledge-Based Systems*, 164:274–291, January 2019. ISSN 0950-7051. doi: 10.1016/j.knosys.2018.10.041. URL <https://www.sciencedirect.com/science/article/pii/S0950705118305343>.
- [25] Wendi Li, Xiao Yang, Weiqing Liu, Yingce Xia, and Jiang Bian. DDG-DA: Data Distribution Generation for Predictable Concept Drift Adaptation. *Proceedings of the AAAI Conference on Artificial Intelligence*, 36(4):4092–4100, June 2022. ISSN 2374-3468. doi: 10.1609/aaai.v36i4.20327. URL <https://ojs.aaai.org/index.php/AAAI/article/view/20327>. Number: 4.

- [26] Yuntao Du, Jindong Wang, Wenjie Feng, Sinno Pan, Tao Qin, Renjun Xu, and Chongjun Wang. AdaRNN: Adaptive Learning and Forecasting of Time Series. In *Proceedings of the 30th ACM International Conference on Information & Knowledge Management, CIKM '21*, pages 402–411, New York, NY, USA, 2021. Association for Computing Machinery. ISBN 978-1-4503-8446-9. doi: 10.1145/3459637.3482315. URL <https://doi.org/10.1145/3459637.3482315>.
- [27] Nikolaos Passalis, Anastasios Tefas, Juho Kannianen, Moncef Gabbouj, and Alexandros Iosifidis. Deep Adaptive Input Normalization for Time Series Forecasting. *IEEE Transactions on Neural Networks and Learning Systems*, PP:1–6, December 2019. doi: 10.1109/TNNLS.2019.2944933.
- [28] Zhiding Liu, Mingyue Cheng, Zhi Li, Zhenya Huang, Qi Liu, Yanhu Xie, and Enhong Chen. Adaptive Normalization for Non-stationary Time Series Forecasting: A Temporal Slice Perspective. *Advances in Neural Information Processing Systems*, 36:14273–14292, December 2023. URL [https://proceedings.neurips.cc/paper\\_files/paper/2023/hash/2e19dab94882bc95ed094c4399cfda02-Abstract-Conference.html](https://proceedings.neurips.cc/paper_files/paper/2023/hash/2e19dab94882bc95ed094c4399cfda02-Abstract-Conference.html).
- [29] Yong Liu, Haixu Wu, Jianmin Wang, and Mingsheng Long. Non-stationary Transformers: Exploring the Stationarity in Time Series Forecasting. In S. Koyejo, S. Mohamed, A. Agarwal, D. Belgrave, K. Cho, and A. Oh, editors, *Advances in Neural Information Processing Systems*, volume 35, pages 9881–9893. Curran Associates, Inc., 2022. URL [https://proceedings.neurips.cc/paper\\_files/paper/2022/file/4054556fcaa934b0bf76da52cf4f92cb-Paper-Conference.pdf](https://proceedings.neurips.cc/paper_files/paper/2022/file/4054556fcaa934b0bf76da52cf4f92cb-Paper-Conference.pdf).
- [30] Jinsung Yoon, W. Zame, and M. Schaar. Multi-directional Recurrent Neural Networks : A Novel Method for Estimating Missing Data. In *Time series workshop in international conference on machine learning*, 2017. URL <https://www.semanticscholar.org/paper/Multi-directional-Recurrent-Neural-Networks-%3A-A-for-Yoon-Zame/77ffd0afe8748e7f241856e517aab45b59634343>.
- [31] Yuan Zhang, Xi Yang, Julie Ivy, and Min Chi. ATTAIN: Attention-based Time-Aware LSTM Networks for Disease Progression Modeling. pages 4369–4375, 2019. URL <https://www.ijcai.org/proceedings/2019/607>.
- [32] Ting Chen, Simon Kornblith, Mohammad Norouzi, and Geoffrey Hinton. A Simple Framework for Contrastive Learning of Visual Representations, June 2020. URL <http://arxiv.org/abs/2002.05709>. arXiv:2002.05709 [cs, stat].
- [33] Aaron van den Oord, Yazhe Li, and Oriol Vinyals. Representation Learning with Contrastive Predictive Coding, January 2019. URL <http://arxiv.org/abs/1807.03748>. arXiv:1807.03748 [cs, stat].
- [34] Vassileios Balntas, Edgar Riba, Daniel Ponsa, and Krystian Mikolajczyk. Learning local feature descriptors with triplets and shallow convolutional neural networks. In *Proceedings of the British Machine Vision Conference 2016*, pages 119.1–119.11, York, UK, 2016. British Machine Vision Association. ISBN 978-1-901725-59-9. doi: 10.5244/C.30.119. URL <http://www.bmva.org/bmvc/2016/papers/paper119/index.html>.
- [35] Aapo Hyvarinen and Hiroshi Morioka. Unsupervised Feature Extraction by Time-Contrastive Learning and Nonlinear ICA. In *Advances in Neural Information Processing Systems*, volume 29. Curran Associates, Inc., 2016. URL [https://proceedings.neurips.cc/paper\\_files/paper/2016/hash/d305281faf947ca7acade9ad5c8c818c-Abstract.html](https://proceedings.neurips.cc/paper_files/paper/2016/hash/d305281faf947ca7acade9ad5c8c818c-Abstract.html).
- [36] Jean-Yves Franceschi, Aymeric Dieuleveut, and Martin Jaggi. Unsupervised Scalable Representation Learning for Multivariate Time Series. In *Advances in Neural Information Processing Systems*, volume 32. Curran Associates, Inc., 2019. URL [https://proceedings.neurips.cc/paper\\_files/paper/2019/hash/53c6de78244e9f528eb3e1cda69699bb-Abstract.html](https://proceedings.neurips.cc/paper_files/paper/2019/hash/53c6de78244e9f528eb3e1cda69699bb-Abstract.html).
- [37] Sana Tonekaboni, Danny Eytan, and Anna Goldenberg. Unsupervised Representation Learning for Time Series with Temporal Neighborhood Coding. In *International Conference on Learning Representations*, October 2020. URL <https://openreview.net/forum?id=8qDwejCuCN>.

- [38] Emadeldeen Eldele, Mohamed Ragab, Zhenghua Chen, Min Wu, Chee Keong Kwoh, Xiaoli Li, and Cuntai Guan. Time-Series Representation Learning via Temporal and Contextual Contrasting. volume 3, pages 2352–2359, August 2021. doi: 10.24963/ijcai.2021/324. URL <https://www.ijcai.org/proceedings/2021/324>. ISSN: 1045-0823.
- [39] Ling Yang and Shenda Hong. Unsupervised Time-Series Representation Learning with Iterative Bilinear Temporal-Spectral Fusion. In *Proceedings of the 39th International Conference on Machine Learning*, pages 25038–25054. PMLR, June 2022. URL <https://proceedings.mlr.press/v162/yang22e.html>. ISSN: 2640-3498.
- [40] Navid Mohammadi Foumani, Lynn Miller, Chang Wei Tan, Geoffrey I. Webb, Germain Forestier, and Mahsa Salehi. Deep Learning for Time Series Classification and Extrinsic Regression: A Current Survey. *ACM Comput. Surv.*, 56(9):217:1–217:45, April 2024. ISSN 0360-0300. doi: 10.1145/3649448. URL <https://dl.acm.org/doi/10.1145/3649448>.
- [41] H. Sakoe and S. Chiba. Dynamic programming algorithm optimization for spoken word recognition. *IEEE Transactions on Acoustics, Speech, and Signal Processing*, 26(1):43–49, 1978. doi: 10.1109/TASSP.1978.1163055.
- [42] Mohammad Shokoohi-Yekta, Jun Wang, and Eamonn Keogh. On the Non-Trivial Generalization of Dynamic Time Warping to the Multi-Dimensional Case. In *Proceedings of the 2015 SIAM International Conference on Data Mining (SDM)*, Proceedings, pages 289–297. Society for Industrial and Applied Mathematics, June 2015. doi: 10.1137/1.9781611974010.33. URL <https://epubs.siam.org/doi/10.1137/1.9781611974010.33>.
- [43] Patrick Schäfer and Ulf Leser. Multivariate Time Series Classification with WEASEL+MUSE, August 2018. URL <http://arxiv.org/abs/1711.11343>. arXiv:1711.11343 [cs].
- [44] David E. Rumelhart, Geoffrey E. Hinton, and Ronald J. Williams. Learning representations by back-propagating errors. *Nature*, 323(6088):533–536, October 1986. ISSN 1476-4687. doi: 10.1038/323533a0. URL <https://www.nature.com/articles/323533a0>. Publisher: Nature Publishing Group.
- [45] Jeffrey L. Elman. Finding Structure in Time. *Cognitive Science*, 14(2):179–211, 1990. ISSN 1551-6709. doi: 10.1207/s15516709cog1402\_1. URL [https://onlinelibrary.wiley.com/doi/abs/10.1207/s15516709cog1402\\_1](https://onlinelibrary.wiley.com/doi/abs/10.1207/s15516709cog1402_1).
- [46] Angus Dempster, François Petitjean, and Geoffrey I. Webb. ROCKET: exceptionally fast and accurate time series classification using random convolutional kernels. *Data Mining and Knowledge Discovery*, 34(5):1454–1495, September 2020. ISSN 1573-756X. doi: 10.1007/s10618-020-00701-z. URL <https://doi.org/10.1007/s10618-020-00701-z>.
- [47] Angus Dempster, Daniel F. Schmidt, and Geoffrey I. Webb. MiniRocket: A Very Fast (Almost) Deterministic Transform for Time Series Classification. In *Proceedings of the 27th ACM SIGKDD Conference on Knowledge Discovery & Data Mining, KDD ’21*, pages 248–257, New York, NY, USA, August 2021. Association for Computing Machinery. ISBN 978-1-4503-8332-5. doi: 10.1145/3447548.3467231. URL <https://doi.org/10.1145/3447548.3467231>.
- [48] Xue Wang, Tian Zhou, Qingsong Wen, Jinyang Gao, Bolin Ding, and Rong Jin. CARD: Channel Aligned Robust Blend Transformer for Time Series Forecasting. In *The Twelfth International Conference on Learning Representations*, October 2023. URL <https://openreview.net/forum?id=MJksr0hurE>.
- [49] Peng Chen, Yingying Zhang, Yunyao Cheng, Yang Shu, Yihang Wang, Qingsong Wen, Bin Yang, and Chenjuan Guo. Pathformer: Multi-scale Transformers with Adaptive Pathways for Time Series Forecasting. In *The Twelfth International Conference on Learning Representations*, October 2023. URL <https://openreview.net/forum?id=1Jk0CMP2aW>.
- [50] Yuxin Li, Wenchao Chen, Xinyue Hu, Bo Chen, Baolin Sun, and Mingyuan Zhou. Transformer-Modulated Diffusion Models for Probabilistic Multivariate Time Series Forecasting. In *The Twelfth International Conference on Learning Representations*, October 2023. URL <https://openreview.net/forum?id=qae04YACHs>.

- [51] Junho Song, Keonwoo Kim, Jeonglyul Oh, and Sungzoon Cho. MEMTO: Memory-guided Transformer for Multivariate Time Series Anomaly Detection. November 2023. URL <https://openreview.net/forum?id=UFW67uduJd>.
- [52] Shengming Zhang, Yanchi Liu, Xuchao Zhang, Wei Cheng, Haifeng Chen, and Hui Xiong. CAT: Beyond Efficient Transformer for Content-Aware Anomaly Detection in Event Sequences. In *Proceedings of the 28th ACM SIGKDD Conference on Knowledge Discovery and Data Mining*, KDD '22, pages 4541–4550, New York, NY, USA, August 2022. Association for Computing Machinery. ISBN 978-1-4503-9385-0. doi: 10.1145/3534678.3539155. URL <https://dl.acm.org/doi/10.1145/3534678.3539155>.
- [53] Shiyang Li, Xiaoyong Jin, Yao Xuan, Xiyong Zhou, Wenhui Chen, Yu-Xiang Wang, and Xifeng Yan. Enhancing the Locality and Breaking the Memory Bottleneck of Transformer on Time Series Forecasting. In *Advances in Neural Information Processing Systems*, volume 32. Curran Associates, Inc., 2019. URL [https://proceedings.neurips.cc/paper\\_files/paper/2019/hash/6775a0635c302542da2c32aa19d86be0-Abstract.html](https://proceedings.neurips.cc/paper_files/paper/2019/hash/6775a0635c302542da2c32aa19d86be0-Abstract.html).
- [54] Jacob Devlin, Ming-Wei Chang, Kenton Lee, and Kristina Toutanova. BERT: Pre-training of Deep Bidirectional Transformers for Language Understanding, May 2019. URL <http://arxiv.org/abs/1810.04805>. arXiv:1810.04805 [cs] version: 2.
- [55] Yuxuan Liang, Kun Ouyang, Yiwei Wang, Xu Liu, Hongyang Chen, Junbo Zhang, Yu Zheng, and Roger Zimmermann. TrajFormer: Efficient Trajectory Classification with Transformers. In *Proceedings of the 31st ACM International Conference on Information & Knowledge Management*, pages 1229–1237, Atlanta GA USA, October 2022. ACM. ISBN 978-1-4503-9236-5. doi: 10.1145/3511808.3557481. URL <https://dl.acm.org/doi/10.1145/3511808.3557481>.
- [56] Haoran Liang, Lei Song, Jianxing Wang, Lili Guo, Xuzhi Li, and Ji Liang. Robust unsupervised anomaly detection via multi-time scale DCGANs with forgetting mechanism for industrial multivariate time series. *Neurocomputing*, 423:444–462, January 2021. ISSN 0925-2312. doi: 10.1016/j.neucom.2020.10.084. URL <https://www.sciencedirect.com/science/article/pii/S0925231220316970>.
- [57] Samira Abnar and Willem Zuidema. Quantifying Attention Flow in Transformers, May 2020. URL <http://arxiv.org/abs/2005.00928>. arXiv:2005.00928 [cs].
- [58] Andre Brown. Eigen Worms Dataset, 2013. URL <https://www.timeseriesclassification.com/description.php?Dataset=EigenWorms>.
- [59] James Large. Ethanol Concentration Dataset, 2018. URL <https://www.timeseriesclassification.com/description.php?Dataset=EthanolConcentration>.
- [60] Rik Henson. Face Detection Dataset, 2014. URL <https://www.timeseriesclassification.com/description.php?Dataset=FaceDetection>.
- [61] Mohammad Shokoohi-Yekta. Handwriting Dataset, 2017. URL <https://www.timeseriesclassification.com/description.php?Dataset=Handwriting>.
- [62] A Goldberger. Heartbeat Dataset, 2016. URL <https://www.timeseriesclassification.com/description.php?Dataset=Heartbeat>.
- [63] M Kudo. Japanese Vowels, 1999. URL <https://www.timeseriesclassification.com/description.php?Dataset=JapaneseVowels>.
- [64] F Alimoglu. Pen Digits Dataset, 1996. URL <https://www.timeseriesclassification.com/description.php?Dataset=PenDigits>.
- [65] Marco Cuturi. PEMS-SF, 2009. URL <https://www.timeseriesclassification.com/description.php?Dataset=PEMS-SF>.
- [66] Thilo Hinterberger. Self Regulation SCP 1 Dataset, 1999. URL <https://www.timeseriesclassification.com/description.php?Dataset=SelfRegulationSCP1>.

- [67] Thilo Hinterberger. Self Regulation SCP 2 Dataset, 1999. URL <https://www.timeseriesclassification.com/description.php?Dataset=SelfRegulationSCP2>.
- [68] N Hammami. Spoken Arabic Digits Dataset, 2010. URL <https://www.timeseriesclassification.com/description.php?Dataset=SpokenArabicDigits>.
- [69] Jiayang Liu. U Wave Gesture Library, 2009. URL <https://www.timeseriesclassification.com/description.php?Dataset=UWaveGestureLibrary>.
- [70] Yu Zheng, Hao Fu, Xing Xie, Wei-Ying Ma, and Quannan Li. *Geolife GPS trajectory dataset - User Guide*. Geolife gps trajectories 1.1 edition, July 2011. URL <https://www.microsoft.com/en-us/research/publication/geolife-gps-trajectory-dataset-user-guide/>.
- [71] Attila Reiss and Didier Stricker. Introducing a New Benchmarked Dataset for Activity Monitoring. In *2012 16th International Symposium on Wearable Computers*, pages 108–109, June 2012. doi: 10.1109/ISWC.2012.13. URL <https://ieeexplore.ieee.org/document/6246152>. ISSN: 2376-8541.
- [72] Denis Kwiatkowski, Peter C. B. Phillips, Peter Schmidt, and Yongcheol Shin. Testing the null hypothesis of stationarity against the alternative of a unit root: How sure are we that economic time series have a unit root? *Journal of Econometrics*, 54(1):159–178, October 1992. ISSN 0304-4076. doi: 10.1016/0304-4076(92)90104-Y. URL <https://www.sciencedirect.com/science/article/pii/030440769290104Y>.
- [73] Yin-Wong Cheung and Kon S. Lai. Lag Order and Critical Values of the Augmented Dickey–Fuller Test. *Journal of Business & Economic Statistics*, 13(3):277–280, July 1995. ISSN 0735-0015. doi: 10.1080/07350015.1995.10524601. URL <https://doi.org/10.1080/07350015.1995.10524601>. Publisher: ASA Website.
- [74] Satya Narayan Shukla and Benjamin Marlin. Interpolation-Prediction Networks for Irregularly Sampled Time Series. September 2018. URL <https://openreview.net/forum?id=r1efr3C9Ym>.
- [75] Hoang Anh Dau, Eamonn Keogh, Kaveh Kamgar, Chin-Chia Michael Yeh, Yan Zhu, Shaghayegh Gharghabi, Chotirat Ann Ratanamahatana, Yanping, Bing Hu, Nurjahan Begum, Anthony Bagnall, Abdullah Mueen, and Gustavo Batista. The UCR Time Series Classification Archive, October 2018. URL [https://www.cs.ucr.edu/~eamonn/time\\_series\\_data\\_2018/](https://www.cs.ucr.edu/~eamonn/time_series_data_2018/).
- [76] Anthony Bagnall, Hoang Anh Dau, Jason Lines, Michael Flynn, James Large, Aaron Bostrom, Paul Southam, and Eamonn Keogh. The UEA multivariate time series classification archive, 2018, October 2018. URL <http://arxiv.org/abs/1811.00075>. arXiv:1811.00075 [cs, stat].
- [77] Dheeru Dua and Casey Graff. UCI Machine Learning Repository, 2017. URL <https://archive.ics.uci.edu/>.
- [78] Dezhi Hong, Jorge Ortiz, Kamin Whitehouse, and David Culler. Towards Automatic Spatial Verification of Sensor Placement in Buildings. In *Proceedings of the 5th ACM Workshop on Embedded Systems For Energy-Efficient Buildings*, BuildSys ’13, pages 1–8, New York, NY, USA, November 2013. Association for Computing Machinery. ISBN 978-1-4503-2431-1. doi: 10.1145/2528282.2528302. URL <https://doi.org/10.1145/2528282.2528302>.
- [79] Laurens van der Maaten and Geoffrey Hinton. Visualizing Data using t-SNE. *Journal of Machine Learning Research*, 9(86):2579–2605, 2008. ISSN 1533-7928. URL <http://jmlr.org/papers/v9/vandermaaten08a.html>.